Geometric and Chelation Influences on the Electronic Structure and Optical Properties of Tetra(carboxylic acid)phenyleneethynylene Dyes

ARTICLE *in* THE JOURNAL OF PHYSICAL CHEMISTRY A · JUNE 2008

Impact Factor: 2.69 · DOI: 10.1021/jp077692z · Source: PubMed

3 AUTHORS:

Asher Berlin
University of Chicago
11 PUBLICATIONS **133** CITATIONS
SEE PROFILE

Chad Risko
University of Kentucky
93 PUBLICATIONS **2,554** CITATIONS
SEE PROFILE

Mark A. Ratner
Northwestern University
905 PUBLICATIONS **42,254** CITATIONS
SEE PROFILE

Geometric and Chelation Influences on the Electronic Structure and Optical Properties of Tetra(carboxylic acid)phenyleneethynylene Dyes

Asher Berlin, Chad Risko,* and Mark A. Ratner

Department of Chemistry, Northwestern University, Evanston, Illinois 60208

Received: September 25, 2007; In Final Form: February 19, 2008

A quantum-chemical study on the consequences of geometric modification and chelation on the electronic structure and optical properties of a tetra(carboxylic acid)phenyleneethynylene dye, of interest for chemical sensing applications, is presented. Rotation within the central biphenylene and complexation with divalent metal ions − in particular Cu^{2+} − lead to notable changes in the absorption and emission profiles. Calculations at both the density functional theory (DFT) and Hartree−Fock (HF) levels are used to evaluate geometric potential energy surfaces for rotation within the central biphenylene unit; HF coupled with configuration interaction singles (HF−CIS) is used to investigate the first excited state of the dye. Time-dependent DFT (TDDFT) calculations are employed to assess changes in optical absorption and fluorescence as a function of geometry and chelation.

I. Introduction

The extended conjugation provided by aryleneethynylene structures is of interest in a number of applications, including the investigation of conductance and switching in single-molecule electronics;[1,2] the design of electroluminescent and photoconductive materials for organic electronics,[3,4] including those that contain transition-metal complexes;[5] and as biological probe fluorophores.[4] In these applications, the geometric conformation of the aryleneethynylene structures plays a significant role in the observed electronic and optical properties. For instance, change in conformation − along with electrostatic charging and tilt − has been postulated as a possible mechanism responsible for voltage-triggered switching.[1] Additionally, locking of the molecular geometric conformation in a rotaxane assembly has been shown to improve chemical stability, electroluminescence efficiency, and fluorescence quantum yields in solution;[4,6] rotaxane structures provide this improved chemical and physical performance partly through screening of environmental effects.[7]

In this work, we are interested in a recently reported phenyleneethynylene dye, **1** (see Figure 1), that is encapsulated by cyclodextrin.[4] Although the free and rotaxanated dyes (FD and RD, respectively) have minor absorption and wavelength maxima differences, the fluorescence quantum yield of RD is larger; additionally, the fluorescence quantum yield of FD in aqueous buffer solution was quenched more readily by the presence of divalent metal ions. Our focus, therefore, is on the influence of the constraints imposed by the rotaxane. We examine the ground-state potential energy surface (PES) of **1** at the density functional theory (DFT) and Hartree−Fock (HF) levels to determine the consequences of geometric modifications on the electronic structure and optical properties. We additionally investigate the effects of deprotonation and binding of divalent metal ions. To gain perspective on the fluorescence properties of **1**, we use HF coupled to configuration interaction singles (CIS) to locate the adiabatic minimum geometry of the first excited state. For comparison, we examine **2** in order to delineate the influence of the carboxylic acid groups on the molecular system.

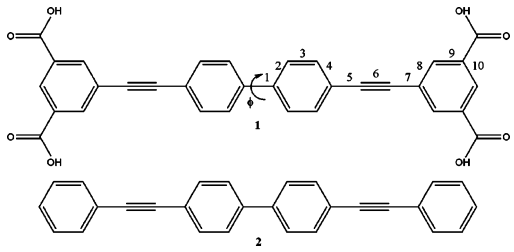

Figure 1. Chemical structures and bond numbering scheme of **1** and **2**.

II. Computational Methodology

Geometry optimizations of **1** and **2** were carried out at both DFT and HF levels with a 6-31G** split valence plus double polarization basis set,[8−10] whereas the deprotonated, closed-shell anion states of **1** (**1**$^{-}$, **1**$^{2-}$, **1**$^{3-}$, **1**$^{4-}$) were evaluated at the DFT level. The DFT calculations were performed with the B3LYP functionals, where Becke's three-parameter hybrid exchange functional[11,12] is combined with the Lee−Yang−Parr correlation functional.[13] To examine steric effects in the RD structure, PESs were determined by freezing the torsion angle between the phenyl rings of the central biphenylene unit at values from 0−90°; the remaining geometric parameters were allowed to relax fully. For the fully optimized and frozen torsion geometries at both the DFT and HF levels, time-dependent DFT (TDDFT) calculations − using both the random-phase and Tamm−Dancoff[14] approximations (RPA and TDA, respectively) − were performed to obtain information pertaining to the vertical electronic excitations. The first-excited-state geometries of **1** and **2** were located using HF−CIS; subsequent TDDFT calculations on the excited-state geometries were performed to estimate the fluorescence properties. Metal-coordinated systems (**Mg1**, **Ca1**, and **Cu1**) were also evaluated at the DFT, HF, and HF−CIS levels of theory; the LANL2DZ effective core potential was used for Cu.[15] All DFT, HF, HF−CIS, and TDDFT calculations were performed with Q-Chem (version 2.0).[16]

* Corresponding author. E-mail: risko@northwestern.edu.

10.1021/jp077692z CCC: $40.75
Published on Web 04/10/2008

TABLE 1: Optimized Bond Lengths (Å) for the Ground States (S_0) of 1 and 2 at Both the B3LYP/6-31G and HF/6-31G** Levels (see Figure 1 for bond numbering scheme) and the First Excited States (S_1) of 1 and 2 at the HF−CIS/6-31G** Level. Δ(1−2) Values for Each Level of Theory**

	S_0						S_1		
	DFT			HF			HF−CIS		
bond (Å)	**1**	**2**	**Δ(1−2)**	**1**	**2**	**Δ(1−2)**	**1**	**2**	**Δ(1−2)**
1	1.481	1.481	0.000	1.489	1.489	0.000	1.427	1.427	0.000
2	1.406	1.406	0.000	1.393	1.393	0.000	1.439	1.439	0.000
3	1.389	1.389	0.000	1.381	1.381	0.000	1.361	1.361	0.000
4	1.409	1.409	0.000	1.392	1.393	−0.001	1.419	1.420	0.001
5	1.423	1.423	0.000	1.439	1.439	0.000	1.415	1.414	−0.001
6	1.216	1.217	−0.001	1.191	1.192	−0.001	1.199	1.200	0.001
7	1.424	1.425	−0.001	1.439	1.440	−0.001	1.433	1.434	0.001
8	1.407	1.410	−0.003	1.391	1.393	−0.002	1.394	1.396	0.002
9	1.398	1.392	0.006	1.388	1.383	0.005	1.387	1.382	−0.005
10	1.398	1.397	0.001	1.387	1.386	0.001	1.388	1.387	−0.001
φ	38.9	38.9	0.0	44.0	44.0	0.0	2.0	1.5	−0.5

TABLE 2: Selected Valence Molecular Orbital Energies (eV) for 1 and 2 at the B3LYP/6-31G and HF/6-31G** (italics) Levels, and E_g (HOMO−LUMO) for Each Structure**

	HOMO-3	HOMO-2	HOMO-1	HOMO	LUMO	LUMO+1	LUMO+2	LUMO+3	E_g
1	−7.31	−7.30	−6.42	−5.85	−2.14	−1.86	−1.86	−1.71	3.71
	−9.62	*−9.58*	*−8.59*	*−7.82*	*1.50*	*1.96*	*1.96*	*2.05*	*9.32*
2	−6.95	−6.95	−5.95	−5.44	−1.70	−1.04	−0.24	−0.15	3.74
	−9.25	*−9.25*	*−8.11*	*−7.44*	*1.91*	*2.73*	*3.73*	*3.74*	*9.35*
Mg1	−6.87	−6.87	−6.70	−6.12	−2.72	−2.54	−2.51	−2.41	3.40
Ca1	−6.47	−6.47	−6.42	−5.87	−2.52	−2.50	−2.36	−2.10	3.35
Cu1	−7.16	−7.10	−6.99	−6.67	−5.09	−3.27	−2.86	−1.99	1.58

III. Results and Discussion

Selected geometric parameters of the DFT and HF optimized geometries for the neutral ground states (S_0) of **1** and **2** are provided in Table 1 with reference bond numbering given in Figure 1. The DFT geometries of **1** and **2** are nearly identical; such similarity indicates that the carboxylic acids have little impact on the π-conjugated structure. The carbon−carbon bond between the phenylene rings in the central biphenylene unit is relatively long at 1.481 Å; the torsion angle between these phenylene rings is 38.9°. Through the carbon backbone of the remaining structure, the phenylene rings show the bond-length alternation (BLA) pattern[17] expected for substituted aromatic structures. The ethynylene segments have a great deal of BLA, with the triple bond being 1.216 Å and the single bond on the order of 1.424 Å. The HF-evaluated S_0 states of **1** and **2** show some deviation versus the DFT geometries, though the patterns are similar. The carbon−carbon bond in the central biphenylene segment is somewhat longer at 1.489 Å, and the biphenylene torsion is more pronounced at 44.0°. The carbon−carbon bonds in the phenylene rings are shorter than those defined at the DFT level and show a smaller BLA pattern. The ethynylene units have a much larger BLA, as the triple bond at the HF level of theory is shorter (1.191 Å) and the single bonds longer (1.439 Å).

Because steric interactions in a rotaxane assembly forces the phenyleneethynylene structure **1** to lose some of its geometric flexibility,[4] we followed the effects of geometry on the electronic structure and subsequent optical properties of the system. Potential energy surfaces for rotation about the biphenylene torsional angle φ at both the B3LYP/6-31G** and HF/6-31G** levels are shown in Figure 2; the associated geometric parameters are listed in Tables S1 and S2 in the Supporting Information. As might be suggested by the ground state calculations, the potential energy surfaces at the DFT and HF levels differ slightly, though the relative trends are similar. For energy differences less than *kT* at room temperature (∼0.6 kcal/mol), the B3LYP/6-31G** calculations predict that torsions of approximately 25−50° are easily accessible, and the HF calculations with the same basis set predict a slightly larger range of approximately 30−60°. The chief difference between the two methodologies has to do with the rise out of the respective surface minima toward either a fully planar (180°) or twisted (90°) conformation. The DFT methodology predicts a sharp rise in energy as the molecule moves toward the fully twisted conformation, whereas the HF energies rise as the geometry shifts toward the planar structure. These differences reflect a common problem when comparing DFT and HF methodologies: due to the inherent self-interaction error that allows an electron to repel itself, DFT methods tend to favor delocalized solutions, while the neglect of electron correlation effects in HF methods can lead to localized solutions;[18−23] the DFT calculations, therefore, tend toward the more planar structure as the HF calculations favor the fully twisted structure.

Geometric parameters for the first-excited states (S_1) of **1** and **2**, as determined at the HF−CIS/6-31G** level, are provided in Table 1. As with the S_0 states, differences in the S_1 states of **1** and **2** are minimal. The biphenylene unit, as has been shown previously for biphenyl-containing compounds,[24,25] virtually planarizes in the S_1 state. The planarization causes a shortening in the biphenylene-bridged carbon−carbon bond to 1.427 Å as the BLA in the phenylene rings move toward a quinoidal structure. The shifts in bond lengths do not extend into the external ethynylene-phenylene unit; the first carbon−carbon bond decreases in length versus the S_0 state, but the remaining carbon−carbon bonds do not change much. The results point to partial localization of the molecular excited state, a situation known for highly conjugated molecules/oligomers.[26]

Selected geometric parameters of the deprotonated anion states − the precursor states for the metal-complexed species in aqueous environments − at the B3LYP/6-31G** level can be found in Table S3 of the Supporting Information. Deprotonation of a single carboxylic acid group introduces a slight asymmetry to the molecular structure that is predominately localized in the phenylene ring containing the carboxyl group;

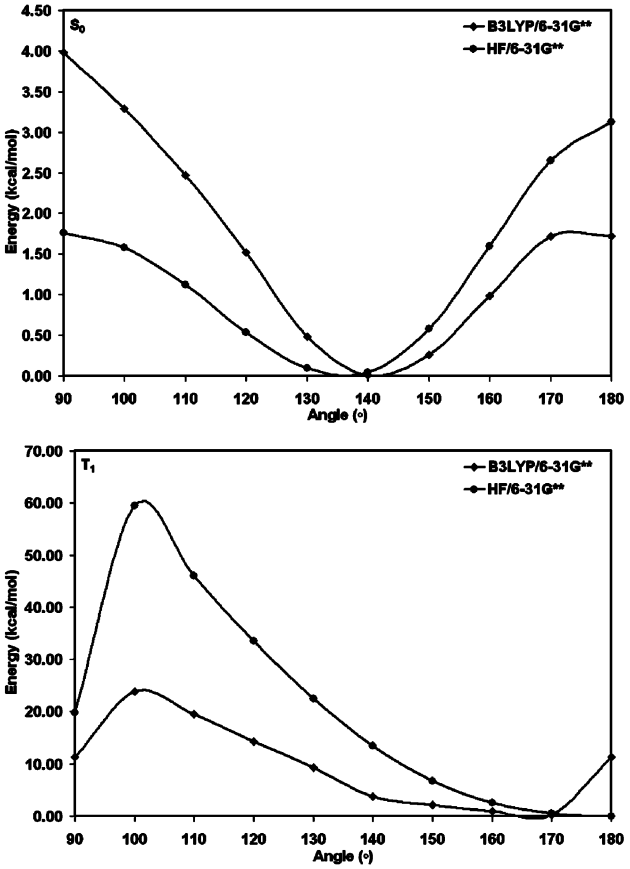

Figure 2. Potential energy surface for rotation about the angle φ in **1** in the S_0 and T_1 electronic states at the B3LYP/6-31G** and HF/6-31G** levels.

the remaining bond lengths are similar to those found in the equilibrium geometry of the neutral ground-state, and the biphenylene torsion is essentially unchanged. Three positional isomers are possible upon bis-deprotonation: a geminally deprotonated structure where deprotonation occurs for carboxylic acid groups on the same phenylene ring, and two vicinally deprotonated structures where deprotonation is either cisoid or transoid about the long molecular axis. In the present gas-phase calculations, the vicinal transoid isomer is the most stable, with the vicinal cisoid isomer slightly higher in energy (0.21 kcal/mol); the geminally deprotonated isomer, on the other hand, is considerably energy destabilized (∼37 kcal/mol). These relative energies point to the ability of the vicinal isomers to distribute the charge associated with the dianion about the entire molecule, while the charge in the geminal structure is forced to be localized on one side of the molecular structure. In aqueous solutions, however, especially in the presence of divalent complexing ions, the deprotonation patterns may be significantly different. From a geometric standpoint, the two vicinal structures possess nearly identical bond lengths and the biphenylene torsion is 38.1°; the geminal structure shows more deviation in bond length with the biphenylene torsion reduced to 35.5°.

Continued deprotonation to the tris-deprotonated structure, as in the case of mono-deprotonation, causes a break in the overall molecular symmetry. There are distinct but small bond length differences in the mono-deprotonated and bis-deprotonated sides of the molecular system; the biphenylene torsion is 35.2°. Full deprotonation restores the original molecular symmetry. We note that − even including the modest change of the biphenylene torsion from 38.9° in the neutral, ground-state structure to 36.8° in the fully deprotonated form − the geometric

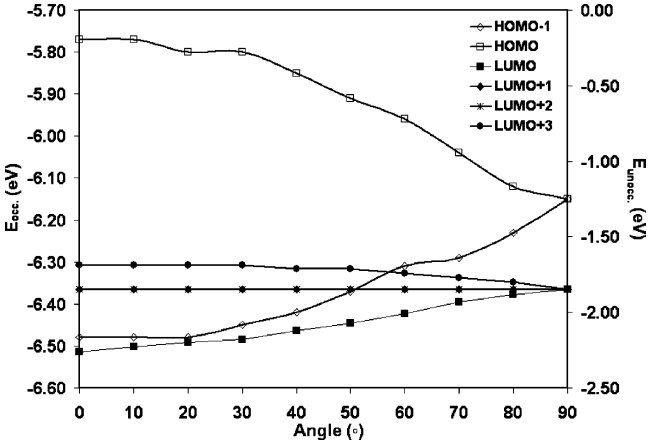

Figure 3. Energies of selected valence occupied (E_{occ}) and unoccupied (E_{unocc}) as a function of biphenylene torsion angle for **1** at the B3LYP/6-31G** level.

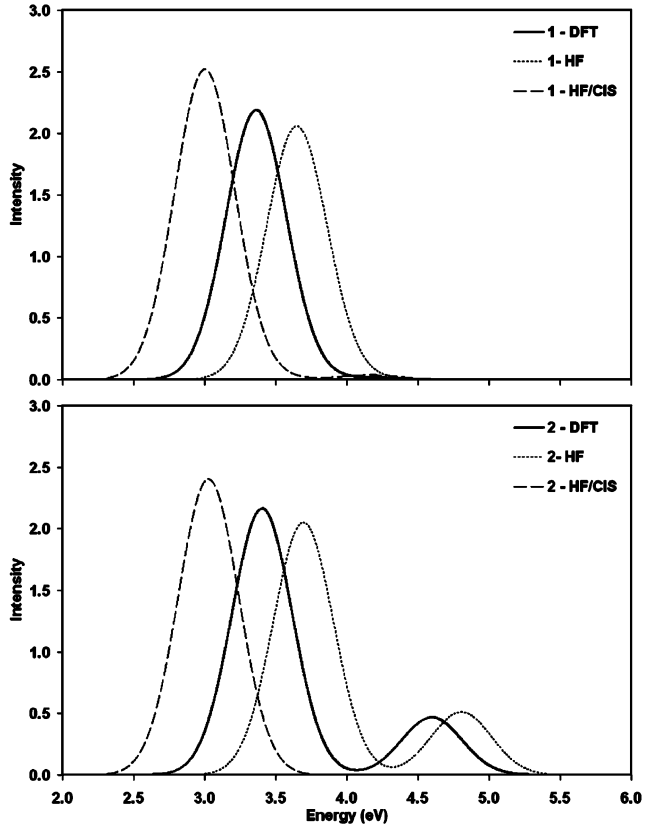

Figure 4. TDDFT (B3LYP/6-31G**) theoretical absorption (— DFT geometry; ··· HF geometry) and emission spectra (- - - HF−CIS geometry) for **1** (top) and **2** (bottom). Gaussian fits of the TDDFT vertical excitations were carried out with a full-width at half-maximum of 0.5 eV.

changes incurred by **1** upon losing four protons are minimal. As expected from simple Coulomb arguments for the series of deprotonations, the removal of the initial hydrogen atom is by far the easiest, with each subsequent step becoming more energetically costly. Recall that these calculations are gas-phase representations of the deprotonated species and do not take into account possible stabilization energies afforded by either solvation or complexation. Recent work by Liptak et al.[27−29] has again shown the (chemically obvious) importance of including solvent effects in determining pK_a with chemical accuracy:[30−47] an error of 1.36 kcal/mol in $\Delta G°$ gives an error

TABLE 3: TDDFT (B3LYP/6-31G) Vertical Absorption Energies (eV), Oscillator Strengths, and Configurations of Excitations**

	energy	oscillation strength[a]	configuration
1	3.36	2.18	HOMO → LUMO (98%)
2	3.40	2.16	HOMO → LUMO (98%)
	4.60	0.42	HOMO-8 → LUMO (8%); HOMO-1 → LUMO+1 (83%)
Mg1	3.07	1.95	HOMO → LUMO (98%)
	3.27	0.12	HOMO-1 → LUMO+1 (5%); HOMO → LUMO+2 (93%)
	4.01	0.41	HOMO-4 → LUMO (6%); HOMO-1 → LUMO+3 (80%)
Ca1	3.01	0.63	HOMO-1 → LUMO+1 (5%); HOMO → LUMO (93%)
	3.17	1.48	HOMO → LUMO+2 (96%)
Cu1	1.33	0.64	HOMO-3 → LUMO (5%); HOMO → LUMO (37%)
	2.55	0.58	HOMO-9 → LUMO (8%); HOMO-5 → LUMO (7%); HOMO-3 → LUMO+1 (4%); HOMO → LUMO+1 (20%); HOMO → LUMO+2 (3%)
	2.78	0.29	HOMO-22 → LUMO (3%); HOMO-9 → LUMO (34%); HOMO → LUMO+1 (6%)
	3.22	0.44	HOMO-18 → LUMO (17%); HOMO-16 → LUMO (3%); HOMO-3 → LUMO+1 (4%); HOMO → LUMO+1 (8%); HOMO → LUMO+2 (8%)
	3.37	0.21	HOMO-32 → LUMO (5%); HOMO-21 → LUMO (22%); HOMO-18 → LUMO (3%); HOMO-3 → LUMO+1 (4%); HOMO → LUMO+1 (4%)

[a] Transitions with oscillator strengths greater than 0.1 are listed.

of 1 pK_a unit.[27] Energies appropriate for comparison with reactions in solution clearly must take into account solvation effects.

Formation of Mg^{2+} and Ca^{2+} complexes introduces minor geometric changes throughout the majority of the π-conjugated molecular structure; see Table S4 in the Supporting Information. The external phenylene rings do undergo a distortion from planarity − on the order of 3−5° − to allow for the complexation of the divalent metal ions by the carboxylate anions; the distortion "lifts" the outermost hydrogen from direct interaction with the metal ion to provide closer contact with the carboxylate units. The metal−oxygen bond for the Mg−O interaction is 1.908 Å and that for the Ca−O interaction is 2.140 Å, results that are in line with the relative size of the metal ions; these results are consistent with previous estimates of unidentate-like binding interactions between carboxylate and these divalent metal ions.[48] As with **1** and **2**, the HF-evaluated S_0 states of **Mg1** and **Ca1** show some deviation versus the DFT geometries, though the patterns are similar. Complexation of Cu^{2+}, on the other hand, imposes notable changes on the exterior of the π-conjugated molecular structure in addition to the deplanarization of the external phenylene rings. Although the central biphenylene segment maintains a similar pattern to **Mg1** and **Ca1**, the BLA patterns in the external phenylene rings increase to provide a more quinoidal pattern; reduced BLA is observed in the ethynylene linkages as well, where the single bonds shorten and the triple bond lengthens. The Cu−O bonds are 1.892 Å. The Cu^{2+} metal ions act as stronger electron-withdrawing agents than either Mg^{2+} or Ca^{2+}, and point to differences that could be expected from interactions between a hard Lewis base (carboxylate anion) and either a hard Lewis acid (both Mg^{2+} and Ca^{2+}) or a borderline Lewis acid (Cu^{2+}). Such hard−soft acid−base interactions are of recent theoretical interest and can show basis set and electron correlation dependencies.[49,50]

To detail the sensitivity of the electronic excitations of **1** to geometric modification and complexation, we begin with a description of the electronic states involved in the transitions. Selected valence molecular orbital energies are listed in Table 2, with pictorial representations in Figure S1 of the Supporting Information. The energies of the highest-occupied and lowest-unoccupied molecular orbitals (HOMO and LUMO, respectively) of **1** are energetically stabilized compared to **2**. The HOMO-1, HOMO, and LUMO of **1** and **2** have the same spatial distribution − fully delocalized across the entire carbon molecular structure. However, the degenerate LUMO+1 and LUMO+2 of **1** are localized on the phenylenedicarboxylic acid end groups, while those molecular orbitals in **2** are π*-orbitals; we therefore expect differences in the optical transitions based on these electronic states for the two molecular structures. Similar patterns in eigenvalue energies and wavefunction distribution are observed for the HF/6-31G** calculations.

Molecular orbital energies for the torsionally constrained structures at the B3LYP/6-31G** level are plotted in Figure 3. Starting with the fully planar structure of **1**, the HOMO−LUMO energy gap (E_g) is 3.51 eV, as the molecular orbital shapes and energy patterns are the same as in the equilibrium geometry. As the torsion moves from the planar orientation, E_g increases to a high of 4.30 eV at 90° as the HOMO becomes more energetically stable and the LUMO slightly destabilizes. The energetic stabilization of the HOMO, along with destabilization of the HOMO-1, leads to the formation of a degenerate set of molecular orbitals at 90°; a similar molecular orbital degeneracy is observed for the virtual orbitals as the LUMO becomes energetically degenerate with the LUMO+1 and LUMO+2. Such degeneracy in the HOMO could lead to possible biradicaloid-like character. As a check, the lowest-lying triplet states (T_1) were optimized at both the DFT and HF levels; in addition, the T_1 biphenylene torsional profile was also examined, see Figure 2. Both methodologies indicate that the T_1 states are higher in energy than the S_0 state; for the optimized structures, $\Delta E(T_1-S_0)$ is 2.3 eV for DFT and 1.1 eV for HF. We thus expect limited biradicaloid character (in the gas phase); higher-order, multielectron calculations are necessary, however, to confirm this assertion.

Complexation with Mg^{2+}, Ca^{2+}, and Cu^{2+} brings about changes in the valence molecular orbitals as new orbitals with density on the divalent metal and carboxylate groups are introduced, see Figure S2 in the Supporting Information. For the Mg^{2+} and Ca^{2+} containing chelates, the HOMO and HOMO-1 are dominated by the same π-type orbitals shown in the parent compound. The LUMO of **Mg1** is similar to that of **1**, while the LUMO+1 and LUMO+2 are magnesium-localized orbitals with character of the outermost s-electronic state. For **Ca1**, the relative ordering of these first few unoccupied orbitals switches as the LUMO and LUMO+1 are the localized, isoenergetic s-type metal orbitals and the LUMO+2 is the lowest π*-type orbital of **1**. These results are in line with expected interactions based on the electronic configurations of the metal ions − Mg^{2+} and Ca^{2+} have closed-shell configurations of [Ne]-$3d^0$ and [Ar]$3d^0$, respectively. Such closed-shell configurations lead to very weak crystal field splitting and strong ionic nature

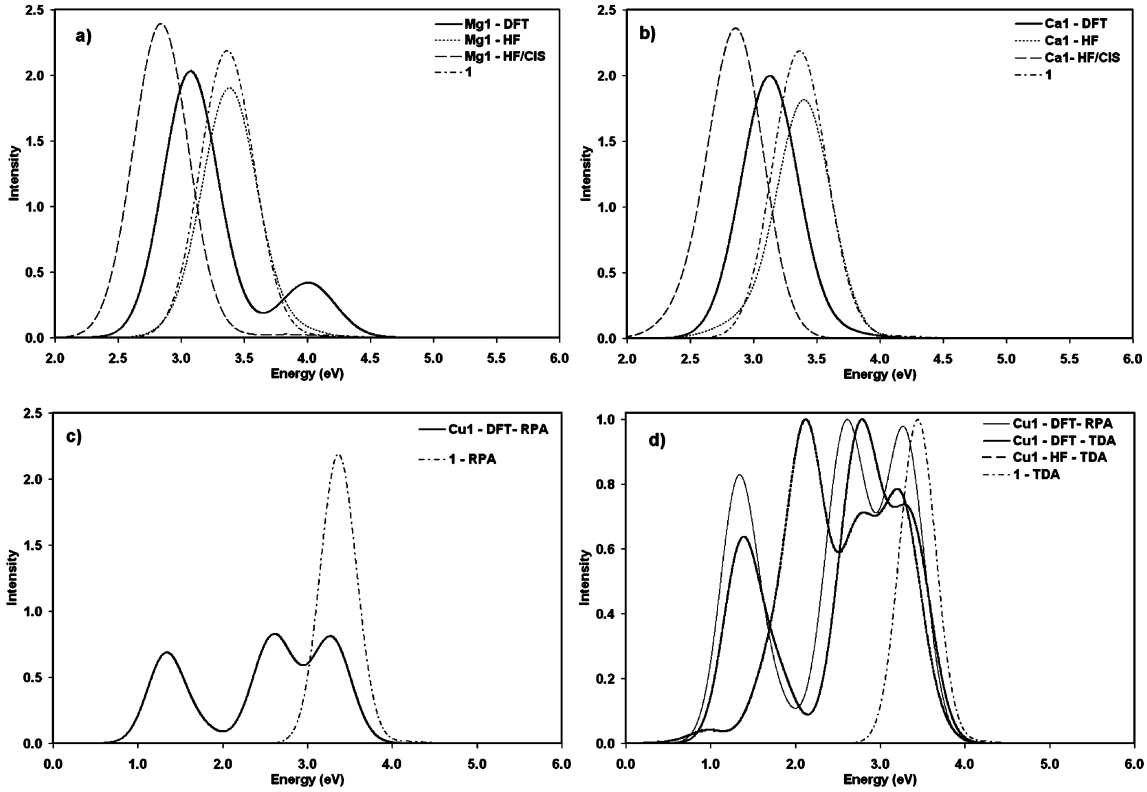

Figure 5. (a) **Mg1** and (b) **Ca1** TDDFT (B3LYP/6-31G**) theoretical absorption (— DFT geometry; ··· HF geometry) and emission spectra (- - - HF−CIS geometry). (c) Comparison of the TDDFT-RPA theoretical absorption spectra for the DFT-optimized geometries of **Cu1** and **1**. (d) Normalized **Cu1** RPA and TDA evaluations of the vertical excitation energies at the DFT (—) and HF (- - -) geometries. The calculated absorption spectrum of **1** is provided for reference. Gaussian fits of the TDDFT vertical excitations were carried out with a full-width at half-maximum of 0.5 eV.

in the bonding between divalent metal ions and carboxylate groups;[51] indeed, analysis of the Mulliken charges reveals a strong ionic interaction along the Mg−O and Ca−O bonds in these structures. The situation for **Cu1**, as might be anticipated for the Cu^{2+} 3d transition metal with an outermost valence electronic configuration of $[Ar]3d^9$,[51] is notably different. Orbitals coupling the exterior phenyelencarboxylate of **1** (LUMO+1 and LUMO+2) with d-orbitals of the metal center are introduced, in turn pushing the π-centered HOMO and LUMO of **1** to the HOMO-3 and LUMO+1 of the Cu^{2+}-chelated compound. Because the HOMO and LUMO are centered about the metal d-orbitals, E_g is dramatically reduced versus the other chelates.

The TDDFT (B3LYP/6-31G**)-determined vertical excitation energies (3.36 eV for **1** and 3.40 eV for **2**) are in relatively good agreement with the empirically derived absorption data for **1** ($\lambda_{abs,max}$ = 3.80 eV [326 nm] in aqueous buffer)[4] and **2** ($\lambda_{abs,max}$ = 4.02 eV [308 nm] in dioxane),[3] see Table 3 (Table S5 in Supporting Information) and Figure 4. The energetic red-shift in the calculated transitions versus experimental data are a common problem for TDDFT methods due to the over-delocalization problem (vide supra); in addition, solvent corrections should be made for a fair comparison. These principal transitions are predominately HOMO → LUMO in nature. TDDFT of the HF/6-31G**-optimized geometries show similar patterns, though the vertical excitation energies are blue-shifted by 0.2 eV, a result of the slight geometric differences between the DFT and HF optimized geometries. Assuming the validity of Kasha's rule[52] for these systems, TDDFT emission energies, calculated on the basis of the HF−CIS/6-31G**-optimized geometries of the lowest excited state, are 3.00 eV for **1** and 3.03 eV for **2**; again, these results are in good agreement with experimental data (3.38 eV [367 nm][4] for **1** and 3.39 eV [366 nm][3] for **2**).

Rotating the biphenylene unit from 0 to 90° induces a blue shift in the main absorption vertical transition energies of **1** (see Table S6 in the Supporting Information) − a shift that corresponds well with the increase in E_g energy as the torsional angle is increased; importantly, there is also considerable change in oscillator strength (from 2.4 at 0° to 1.7 at 80°) along the rotational PES. Likewise, a strong blue shift in the vertical transition energies (see Table S7 in the Supporting Information) and range of oscillator strengths (from 2.5 at 10° to 2.1 at 50°) occurs for the calculated emission profile along the PES. These results help characterize the emission intensity differences between the inclusion of **1** in a rotaxane assembly versus being free in solution:[4] by impeding the free rotation within the biphenylene unit and limiting internal conversion processes, **1** is constrained to lose the absorbed energy through a photon from a sterically hindered geometric configuration rather than via heat through nonradiative (vibrational) decay pathways.

As expected from the changes in the molecular orbital structure, additional transitions appear in the absorption profiles of the chelated structures, see Figure 5. For **Mg1** and **Ca1**, the dominant optical signal is principally composed of the $\pi \rightarrow \pi^*$ transition observed in **1** and **2**; the transitions, though, are red-shifted versus **1**. Near these predominant vertical transitions, lower intensity transitions principally composed of $\pi \rightarrow$ metal charge transfer are found; this transition is blue-shifted by 0.2 eV for **Mg1**, but red-shifted by approximately the same amount for **Ca1**, results in line with the relative energetic ordering of the outermost s-type orbitals of the metal with respect to the lowest π^*-orbital of the dye. There is an additional transition

near 4 eV for **Mg1** that is of $\pi \rightarrow \pi^*$ character. TDDFT of the HF/6-31G**-optimized geometries show similar patterns, though the vertical excitation energies are blue-shifted as in **1** and **2**, a result of the slight geometric differences between the DFT and HF minimum geometries. Analyses of the HF−CIS/6-31G**-optimized first-excited states show that the principal emission peaks are red-shifted to approximately 2.9 eV. These emission peaks are slightly red-shifted (~0.1 eV) versus **1**. This negligible shift in the principal emission peak agrees well with the experimental finding that Mg coordination results in limited emission quenching of the dye without changing the emission frequency.[4]

As noted above, the valence molecular orbital structure of **Cu1** greatly differs versus those of **Mg1** and **Ca1** due to coupling between the Cu^{2+} d-orbitals and the exterior phenyelencarboxylate orbitals of the dye − a difference that in turn alters the nature of the vertical electronic transitions and optical spectrum, see Table 3 and Figure 5. The first TDDFT transition for the DFT ground-state structure − described as HOMO → LUMO − involves the coupled metal-dye exterior orbitals and is located at 1.3 eV; a result in line with the smaller E_g for **Cu1** versus the other chelated structures. In the visible portion of the spectrum, the principal peak near 3 eV observed for the other species is replaced by two lower-intensity bands each comprising two vertical transitions involving a number of metal- and π-centered molecular orbitals; these visible bands are in line with those recently reported for a Cu^{2+}-spiropyran dye complex designed to take advantage of the fluorescence inner filter effect with a porphyrin-based fluorescer.[53] The different valence electronic structure of **Cu1** moreover leads to significant differences in the evaluation of the ground and excited-state minima at the HF and HF−CIS levels of theory. The HF calculations of **Cu1** (in direct contradiction to the other HF evaluations considered herein) gave a planar geometry with similar geometric parameters to that for the S_1 state of **1**, whereas the inclusion of electron correlation through the use of CIS gave the twisted S_0-like structure of **1**. These results (along with the large number of closely spaced Cu d-orbitals intertwined with π-orbitals localized on the dye) point to the need for the extensive treatment of electron correlation through high-level complete active space calculations (e.g., CASSCF) for an accurate determination of the minimum wave function of **Cu1**; indeed, this is already often a necessary step for the proper description of twisted "tictoid" molecular species with close-lying electronic levels.[54,55] In addition, the slight alterations of the minimum HF and HF−CIS geometries versus the DFT structure result in electronic configurations that give imaginary RPA roots in subsequent TDDFT evaluations. Nonetheless, as we are principally interested in describing how Cu^{2+} chelation might shift the absorption and emission spectra of **1**, we can use the TDA results of the minimized geometries for evaluation.[56] Indeed, using the HF structure with the planar biphenylene motif induces a red-shift of the principal transitions of **Cu1** versus the twisted-biphenylene DFT structure. The results for the twisted and planar **Cu1** geometries suggest reasons for both the dramatic decrease in emission intensity and the broadening of the emission line shape for the Cu^{2+}-coordinated dye in ref 4: because the principal **Cu1** transition is located at a significantly lower energy, following Kasha's rule, one would expect the main emission peak of **Cu1** to be at a much lower energy versus **1** resulting in a lower emission intensity for the (unbound) dye in the presence of Cu^{2+} in solution; in addition, the presence of other vertical transitions in the 3−4 eV range for **Cu1** will lead to an overall broadening of the spectrum versus **1**. The above notable changes in the spectra of the metal-complexed species suggest that **1** can be of interest in chemical sensing applications.

IV. Conclusion

We have examined how modifications to the geometric structure and chelation influence electronic structure and optical characteristics of **1**. The PES for rotation within the biphenylene segment shows that rotation between 25 and 50° is freely allowed at room temperature. The electronic structure and absorption properties for geometries in this range vary slightly. The lowest excited-state geometry has a nearly planar biphenylene configuration. Because of the nearly flat potential for rotation within the biphenylene segment, the presence of nonradiative decay pathways has been postulated as the reason that **1** free in solution has a lower emission intensity than its rotaxanated (geometrically constrained) couterpart.[4] Indeed, we have seen a range of transition energies and oscillator strengths for the primary absorption and emission profiles along the PES for rotation in the biphenylene segment that could be frozen out in the sterically hindered RD structure and lead to larger emission intensities versus FD through the limitation of internal conversion pathways. Chelation of **1** with Mg^{2+} and Ca^{2+} alters the geometric structures only slightly, but complexation with Cu^{2+} introduces more significant changes. The electronic structures for these chelated species show orbital density residing on the metal ions that in turn alter the absorption properties by changing the nature of the electronic excitations; in particular, orbital energy ordering changes for the Cu adduct lead to a very strong predicted change in the optical spectrum. These changes result in absorption and emission profile modifications that should allow for the detection of divalent metal ions in sensing applications.

Acknowledgment. The work at Northwestern was supported by the NSF through the Northwestern University MRSEC (DMR-0076097) and the NNI−NCN, and through the MURI/DURINT program of the DoD.

Supporting Information Available: Tables of selected geometric parameters, excited-state energies and electronic configuration, and plots of molecular orbital density (PDF). This material is available free of charge via the Internet at http://pubs.acs.org.

References and Notes

(1) Blum, A. S.; Kushmerick, J. G.; Long, D. P.; Patterson, C. H.; Yang, J. C.; Henderson, J. C.; Yao, Y.; Tour, J. M.; Shashidhar, R.; Ratna, B. R. *Nat. Mater.* **2005**, *4*, 167.

(2) Keane, Z. K.; Ciszek, J. W.; Tour, J. M.; Natelson, D. *Nano Lett.* **2006**, *6*, 1518.

(3) Birckner, E.; Grummt, U. W.; Göller, A. H.; Pautzsch, T.; Egbe, D. A. M.; Al-Higari, M.; Klemm, E. *J. Phys. Chem. A* **2001**, *105*, 10307.

(4) Park, J. S.; Wilson, J. N.; Hardcastle, K. I.; Bunz, U. H. F.; Srinivasaro, M. *J. Am. Chem. Soc.* **2006**, *128*, 7714.

(5) Ley, K. D.; Schanze, K. S. *Coord. Chem. Rev.* **1998**, *171*, 287.

(6) Terao, J.; Tang, A.; Michels, J. J.; Krivokapic, A.; Anderson, H. L. *Chem. Commun.* **2004**, 56.

(7) Stanier, C. A.; O'Connell, M. J.; Clegg, W.; Anderson, H. L. *Chem. Commun.* **2001**, 493.

(8) Francl, M. M.; Petro, W. J.; Hehre, W. J.; Binkley, J. S.; Gordon, M. S.; DeFrees, D. J.; Pople, J. A. *J. Chem. Phys.* **1982**, *77*, 3654.

(9) Hariharan, P. C.; Pople, J. A. *Theor. Chim. Acta* **1973**, *28*, 213.

(10) Rassolov, V. A.; Pople, J. A.; Ratner, M. A.; Windus, T. L. *J. Chem. Phys.* **1998**, *109*, 1223.

(11) Becke, A. D. *Phys. Rev. A: At., Mol., Opt. Phys.* **1988**, *38*, 3098.

(12) Becke, A. D. *J. Chem. Phys.* **1993**, *98*, 5648.

(13) Lee, C.; Yang, W.; Parr, R. G. *Phys. Rev. B: Condens. Matter Mater. Phys.* **1988**, *37*, 785.

(14) Hirata, S.; Head-Gordon, M. *Chem. Phys. Lett.* **1999**, *314*, 291.
(15) Hay, P. J.; Wadt, W. R. *J. Chem. Phys.* **1985**, *82*, 284.
(16) Kong, J.; White, C.; Krylov, A.; Sherrill, D.; Adamson, R.; Furlani, T.; Lee, M.; Lee, A.; Gwaltney, S.; Adams, T.; Ochsenfeld, C.; Gilbert, A.; Kedziora, G.; Rassolov, V.; Maurice, D.; Nair, N.; Shao, Y.; Besley, N.; Maslen, P.; Dombroski, J.; Daschel, H.; Zhang, W.; Korambath, P.; Baker, J.; Byrd, E.; Van Voorhis, T.; Oumi, M.; Hirata, S.; Hsu, C.; Ishikawa, N.; Florian, J.; Warshel, A.; Johnson, B.; Gill, P.; Head-Gordon, M.; Pople, J. *J. Comput. Chem.* **2000**, *21*, 1532.
(17) Marder, S. R.; Gorman, C. B.; Meyers, F.; Perry, J. W.; Bourhill, G.; Brédas, J. L.; Pierce, B. M. *Science* **1994**, *265*, 632.
(18) Bally, T.; Borden, W. T. In *Reviews in Computational Chemistry*; Lipkowitz, K. B., Boyd, D. B., Eds.; Wiley-VCH: Weinheim, Germany, 1999; Vol. 13, p 1.
(19) Pacchioni, G.; Frigoli, F.; Ricci, D. *Phys. Rev. B: Condens. Matter Mater. Phys.* **2000**, *63*, 054102.
(20) Kobko, N.; Masunov, A.; Tretiak, S. *Chem. Phys. Lett.* **2004**, *392*, 444.
(21) Lundberg, M.; Siegbahn, P. E. M. *J. Chem. Phys.* **2005**, *122*, 224103.
(22) Lambert, C.; Risko, C.; Coropceanu, V.; Schelter, J.; Amthor, S.; Gruhn, N.; Durivage, J. C.; Brédas, J. L. *J. Am. Chem. Soc.* **2005**, *127*, 8508.
(23) Coquet, R.; Willock, D. J. *Phys. Chem. Chem. Phys.* **2005**, *7*, 3819.
(24) Imamura, A.; Hoffman, R. *J. Am. Chem. Soc.* **1967**, *90*, 5379.
(25) Im, H. S.; Bernstein, E. R. *J. Chem. Phys.* **1988**, *88*, 7337.
(26) Tretiak, S.; Saxena, A.; Martin, R. L.; Bishop, A. R. *Phys. Rev. Lett.* **2002**, *89*, 097402.
(27) Liptak, M. D.; Shields, G. C. *J. Am. Chem. Soc.* **2001**, *123*, 7314.
(28) Liptak, M. D.; Shields, G. C. *Int. J. Quantum Chem.* **2001**, *85*, 727.
(29) Liptak, M. D.; Gross, K. C.; Seybold, P. G.; Feldgus, S.; Shields, G. C. *J. Am. Chem. Soc.* **2002**, *124*, 6421.
(30) Zhu, X. Q.; Wang, C. H.; Liang, H.; Cheng, J. P. *J. Org. Chem.* **2007**, *72*, 945.
(31) Kelly, C. P.; Cramer, C. J.; Truhlar, D. G. *J. Phys. Chem. B* **2007**, *111*, 408.
(32) Qi, X. J.; Liu, L.; Fu, Y.; Guo, Q. X. *Organometallics* **2006**, *25*, 5879.
(33) da Silva, G.; Kennedy, E. M.; Dlugogorski, B. Z. *J. Phys. Chem. A* **2006**, *110*, 11371.
(34) Kelly, C. P.; Cramer, C. J.; Truhlar, D. G. *J. Phys. Chem. A* **2006**, *110*, 2493.
(35) Eckert, F.; Klamt, A. *J. Comput. Chem.* **2006**, *27*, 11.
(36) Gao, D. Q.; Svoronos, P.; Wong, P. K.; Maddalena, D.; Hwang, J.; Walker, H. *J. Phys. Chem. A* **2005**, *109*, 10776.
(37) Soriano, E.; Cerdan, S.; Ballesteros, P. *J. Mol. Struct.−Theochem* **2004**, *684*, 121.
(38) Schmidt am Busch, M.; Knapp, E. W. *Chem. Phys. Chem.* **2004**, *5*, 1513.
(39) Magill, A. M.; Cavell, K. J.; Yates, B. F. *J. Am. Chem. Soc.* **2004**, *126*, 8717.
(40) Barone, V.; Improta, R.; Rega, N. *Theor. Chem. Acc.* **2004**, *111*, 237.
(41) Dunn, M. E.; Pokon, E. K.; Shields, G. C. *J. Am. Chem. Soc.* **2004**, *126*, 2647.
(42) Fu, Y.; Liu, L.; Li, R. C.; Liu, R.; Guo, Q. X. *J. Am. Chem. Soc.* **2004**, *126*, 814.
(43) Klamt, A.; Eckert, F.; Diedenhofen, M.; Beck, M. E. *J. Phys. Chem. A* **2003**, *107*, 9380.
(44) Saracino, G. A. A.; Improta, R.; Barone, V. *Chem. Phys. Lett.* **2003**, *373*, 411.
(45) Jang, Y. H.; Goddard, W. A.; Noyes, K. T.; Sowers, L. C.; Hwang, S.; Chung, D. S. *J. Phys. Chem. B* **2003**, *107*, 344.
(46) Chipman, D. M. *J. Phys. Chem. A* **2002**, *106*, 7413.
(47) Pliego, J. R.; Riveros, J. M. *J. Phys. Chem. A* **2002**, *106*, 7434.
(48) Nara, M.; Torii, H.; Tasumi, M. *J. Phys. Chem.* **1996**, *100*, 19812.
(49) Chandrakumar, K. R. S.; Pal, S. *J. Phys. Chem. A* **2003**, *107*, 5755.
(50) Mendez, F.; Garcia-Garibay, M. A. *J. Org. Chem.* **1999**, *64*, 7061.
(51) Bala, T.; Prasad, B. L. V.; Sastry, M.; Kahaly, M. U.; Waghmare, U. V. *J. Phys. Chem. A* **2007**, *111*, 6183.
(52) Kasha, M. *Faraday Discuss.* **1950**, *9*, 14.
(53) Shao, N.; Zhang, Y.; Cheung, S. M.; Yang, R. H.; Chan, W. H.; Mo, T.; Li, K. A.; Liu, F. *Anal. Chem.* **2005**, *77*, 7294.
(54) Brown, E. C.; Marks, T. J.; Ratner, M. A. *J. Phys. Chem. B* **2008**, *112*, 44.
(55) Isborn, C. M.; Davidson, E. R.; Robinson, B. H. *J. Phys. Chem. A* **2006**, *110*, 7189.
(56) The TDA and RPA results for the optimized DFT ground state structures of **1** and Cu1 are nearly identical, thus giving credence to the use of TDA for further comparison.